Surface plasmon effects induced by uncollimated emission of semiconductor microstructures

Dominic Lepage and Jan J. Dubowski*

Department of Electrical and Computer Engineering, Center of Excellence for Information Engineering, Université de Sherbrooke, Sherbrooke, Québec J1K 2R1, Canada
** Corresponding author: jan.j.dubowski@usherbrooke.ca*

Abstract: We have recently proposed an innovative microstructure for a monolithically integrated surface plasmon resonance (SPR) device comprising a metal coated SiO_2 layer deposited atop a photoluminescence emitting quantum well (QW) wafer. The functioning of such a device is based on the uncollimated and incoherent emission of semiconductors. We discuss the results of our calculations aimed at the description of SPs coupling in QW semiconductor-based SPR architectures designed for biosensing applications. Two SPs modes could be coupled in the 0^{th} diffraction order where the injected in-plane wavevectors from the QW structures can always meet SPR conditions. This results in increasing the SPs coupling efficiency up to 100 times higher than in case of indirect SPs injection.

OCIS codes: (240.6680) Surface plasmons; (230.0230) Optical devices; (170.4520) Optical confinement and manipulation; (290.0290) Scattering.

References and links

1. R. B. M. Schasfoort, and A. J. Tudos, *Handbook of surface plasmon resonance* (R. Soc. of Chem., Cambridge, 2008).
2. H. Raether, "Surface-Plasmons on smooth and rough surfaces and on gratings," Springer Tracts in Mod. Phys. **111**, 1-133 (1988).
3. D. Lepage, and J. J. Dubowski, "Surface plasmon assisted photoluminescence in GaAs-AlGaAs quantum well microstructures," Appl. Phys. Lett. **91**, 163106 (2007).
4. L. F. Li, "Fourier modal method for crossed anisotropic gratings with arbitrary permittivity and permeability tensors," J. Opt. A: Pure Appl. Opt. **5,** 345-355 (2003)
5. M. G. Moharam, D. A. Pommet, E. B. Grann, and T. K. Gaylord, "Stable implementation of the rigorous coupled-wave analysis for surface-relief gratings-enhanced transmittance matrix approach," J. Opt. Soc. Am. A **12**, 1077-1086 (1995).
6. J. Hench, and Z. Strakos, "*The RCWA method - a case study with open questions and perspectives of algebraic computations*," to appear in ETNA (2009).
7. L. Mashev, and E. Popov, "Reflection gratings in conical diffraction mounting," J. Opt.**18**, 3-7 (1987).
8. E. Takeda, T. Nakamura, M. Fujii, S. Miura, and S. Hayashi, "Surface plasmon polariton mediated photoluminescence from excitons in silicon nanocrystals," Appl. Phys. Lett. **89**, 101907 (2006).
9. D. Amans, S. Callard, A. Gagnaire, J. Joseph, G. Ledoux, and F. Huisken, "Ellipsometric study of silicon nanocrystal optical constants," J. Appl. Phys. **93**, 4173-4179 (2003).
10. G. V. Prakash, M. Cazzanelli, Z. Gaburro, L. Pavesi, F. Iacona, G. Franzo, and F. Priolo, "Linear and nonlinear optical properties of plasma-enhanced chemical-vapour deposition grown silicon nanocrystals," J. Mod. Opt. **49**, 719-730 (2002).
11. E. D. Palik, *Handbook of optical constants of solids* (Academic Press, Orlando, 1985).
12. M.-L. Thèye, "Investigation of the Optical Properties of Au by Means of Thin Semitransparent Films," Phys. Rev. B **2**, 3060-3078 (1970).

#111139 - $15.00 USD Received 8 May 2009; revised 2 Jun 2009; accepted 3 Jun 2009; published 5 Jun 2009

13. S. Patskovsky, M. Vallieres, M. Maisonneuve, I. H. Song, M. Meunier, and A. V. Kabashin, "Designing efficient zero calibration point for phase-sensitive surface plasmon resonance biosensing," Opt. Express **17**, 2255-2263 (2009).

1. Introduction

The inherent surface sensitivity of the surface plasmon resonance (SPR) effect has made it highly attractive for biochemical analysis of processes localized on metal surfaces. Many SPR devices have been developed and made commercially available for that purpose in the past 20 years[1]. However, most of them are relatively bulky and a monolithically integrated SPR microchip, which could be easily included in specimen processing hardware for a wholly automated analysis, has yet to be demonstrated. A first step towards this integration would be embedding a light source in a microstructure designed for SPR. Strong photoluminescence (PL) from some bulk semiconductor materials or their microstructures in form of thin films, quantum well (QW), quantum dot (QD), and arrays of nano-crystals (NCs) makes them attractive for developing monolithically integrated SPR devices.

A thin dielectric-metal-dielectric (DMD) microstructure deposited on top of a PL emitting semiconductor could provide conditions suitable for surface plasmons (SPs) formation and observation of a variety of bio-chemical reactions. Because of the proximity and the nature of the materials involved, the light injected in such a system is uncollimated and usually incoherent. As illustrated in Fig. 1, any given point of a metallic layer in the DMD microstructure will be exposed to the whole wavevector spectrum (angles of emission) and couple all SPR modes possibly supported by the architecture for the excited energies. While a constant light intensity is measured at a given plane of the real-space, every supported photonic mode is induced in the Fourier-space (k_{ll}).

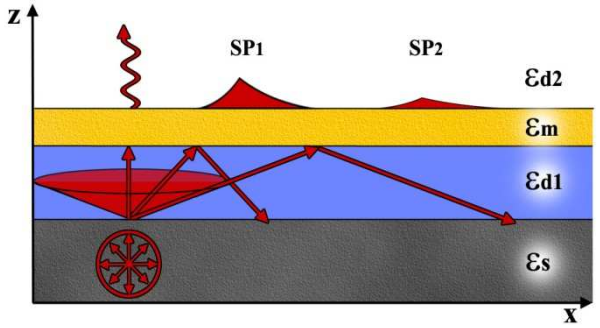

Fig. 1. The embedded semiconductor (ε_s) emits an uncollimated and usually incoherent light. At fixed energy, the DMD interface (ε_{d2} - ε_m - ε_{d1}) is exposed to a continuous range of wavevector excitation, coupling all the SPR modes possibly supported by the architecture. Since the whole semiconductor layer (ε_s) emits in the depicted manner, a constant light intensity is measured in the real space, while all SPs modes can be excited in the Fourier space (k_{ll}). If the light source emits a broad energy spectrum, a continuum of dispersion relations $\omega(k_{ll})$ can be met.

In addition, most embedded semiconductor light sources will have a relatively large emission spectra (from ±50nm in QW to ±100nm in NCs), thus they will simultaneously generate a continuum of SPs dispersion relation ω(kll) (angular frequency versus in-plane wavevectors). This case is different from the traditional "macro" SPs coupling case, where one energy is considered and one wavevector is injected by the irradiating laser [1, 2]. We have recently reported on the measurements of SP effects in a DMD microstructure comprising SiO2–Au deposited on top of a PL emitting GaAs-Al0.5Ga0.5As QW microstructures [3]. The extraction of SPs in these microstructures was achieved with a short-

#111139 - $15.00 USD Received 8 May 2009; revised 2 Jun 2009; accepted 3 Jun 2009; published 5 Jun 2009

period grating fabricated within the Au layer. However, only a semi-qualitative interpretation of the results could be provided due to the lack of an analytical tool capable of predicting the full behaviour of the observed effects. In this communication, we discuss the results of our calculations aimed at the description of surface plasmons generated in DMD microstructures monolithically interfaced with self-emitting semiconductor architectures.

2. Semiconductor light sources for SPR

The calculations were carried out using a Rigorous Coupled-Wave Analysis (RCWA) algorithm and scattering matrices approach [4, 5]. This allowed us to predict the coupling of semiconductor photoluminescence (PL) to SP generating architectures and describe the propagation of SPs in both the Near- and Far-Fields. Scattering matrices / RCWA approach was preferred in these case because it has been shown to be remarkably robust: for arbitrary shapes, it is able to reliably compute the electromagnetic field distribution for any wavelengths and incidence angles [4-6], even for conical diffraction mounting [7]. The studied architectures consist of layered dielectrics, which simplify even further the required calculations by reducing the dimensionality of the problem and designate RCWA as a perfect candidate for analytic solutions. The gratings presented are considered semi-infinite over the specified dimension as the sample ($1cm^2$) and grating regions ($1mm^2$) are much larger than the employed wavelengths (IR) and SPs propagation lengths (μm scales). The computation time of the method is also attractive for efficient architecture designing, with the allotted time for the solution of the inverse problem typically between 2 and 10 seconds (solver and hardware dependent). For a given architecture, a set of variables, such as energies, angles, spatial positions (Near- and Far-Fields) or dielectric thicknesses are solved simultaneously through tensor algebra. A 2D or 3D slice of the solution, such as Near-Field spatial distribution or a dispersion relation map $\omega(k_{ll})$, can then be presented in the form of a plot. All the calculations are done using a standard PC (Intel® Core Duo™ CPU, 2.33 GHz, 1.95 GB RAM) using MATLAB® language.

An initial verification of the developed analytical tools was performed for a microstructure comprising a 200-nm-thick layer of silicon nanocrystals (Si-NCs) grown on SiO_2 [8]. A 189-nm-thick 765-nm-period sinusoidal photoresist (PR) grating was constructed on top of a 50-nm-thick layer of Au that covered Si-NCs . While the Si-NCs are pumped from the back of the silica with a 488nm laser, the emitted PL is measured in transmission through the whole architecture. Fig. 2 presents the calculated dispersion relation $\omega(k_{ll})$ for the whole architecture as diffracted in the far-field. Only the 1st diffraction order is presented for clarity. The spectrum is modulated by the Si-NCs PL emission. The white dots are the local maxima experimentally measured in the original paper [8]. Up to a 10% error should be added to these results from the NA of the setup (inducing a $\pm 1^o$ uncertainty). The dashed lines follow the calculated local maxima for the surface plasmon polaritons (SPP) resonance modes (for both the Au/ Si-NCs and Au/PR interfaces). Since the energy dependent dielectric constants of the Si-NCs were not characterized, we used a range of values presented in literature [9, 10]. The PR refractive index was fixed at 1.68 as in [8], the fused silica refractive indices were taken from [11] and those for gold from experimentally determined measurements for e-beam evaporated thin films [11, 12].

#111139 - $15.00 USD Received 8 May 2009; revised 2 Jun 2009; accepted 3 Jun 2009; published 5 Jun 2009

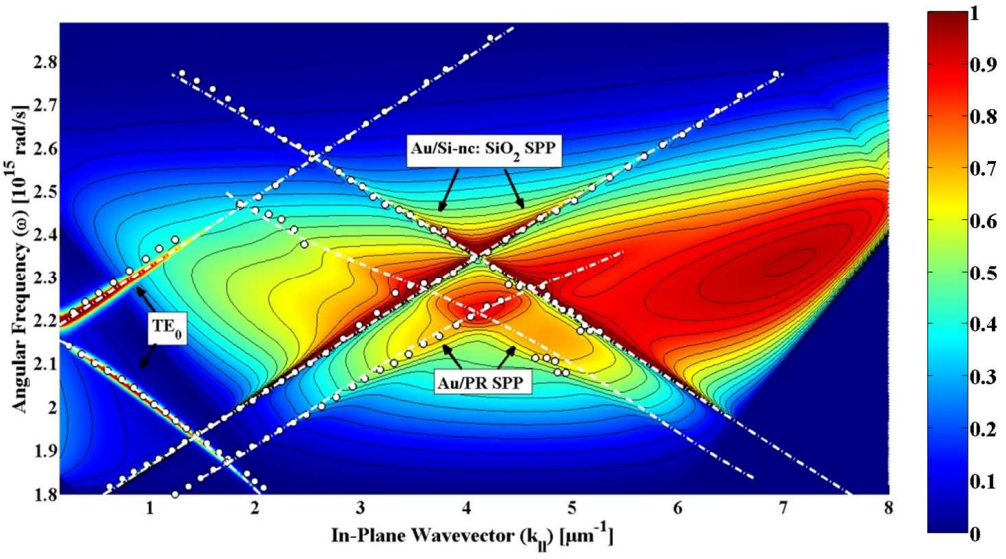

Fig. 2. Calculated dispersion relation $\omega(k_{ll})$ of the Si-NCs architecture in the 1st diffraction order as observed in the far-field. White lines follow the analytical SPR peaks from the Au/ Si-NCs SPP, the Au/ PR SPs and the TE_0 mode. White dots are experimental results from [8]. The intensity is modulated by the Si-NCs emission and normalized to one.

As presented on Fig. 2, the calculations are in very good agreement with the experiment. The dashed curves accurately predict the measured peaks of Au/Si-NCs and Au/PR SPP along with the TE mode in the thick PR layer (189nm). Higher PL intensities are predicted for $\omega(k_{ll})$ where SP modes meet. Moreover, measured points straying away from the resonance lines are actually expected to follow the calculated equipotential lines of PL intensity, as clearly illustrated in the Fig. Here, the analytical predictions are in better agreement than originally presented [8] because SPP is not the only effect taken into account in our calculations of the Far-Field intensity distribution. Sums of other phenomena, such as the architecture's transmittance, the guided modes and the photonic bandgaps are taken into account in our analytical approach. This has allowed us to predict more accurately the experimental values of PL peak intensities.

Figure 3(a) shows the calculated dispersion relation $\omega(k_{ll})$ for the SPR architecture comprising a PL emitting GaAs-AlGaAs heterostructure coated with a 326-nm-thick layer of SiO_2 and a 10-nm-thick layer of Au. A 372nm square grating (0.45 duty cycle) of 20nm Au was fabricated on top of that microstructure using e-beam lithography. The architecture was protected by a 100nm-thick layer of PR [3]. Only the 1st diffraction order is presented for clarity and comparison purposes. The calculations were carried out for the transmitted far-field PL intensity, unmodulated by the QW PL emisssion.

#111139 - $15.00 USD Received 8 May 2009; revised 2 Jun 2009; accepted 3 Jun 2009; published 5 Jun 2009

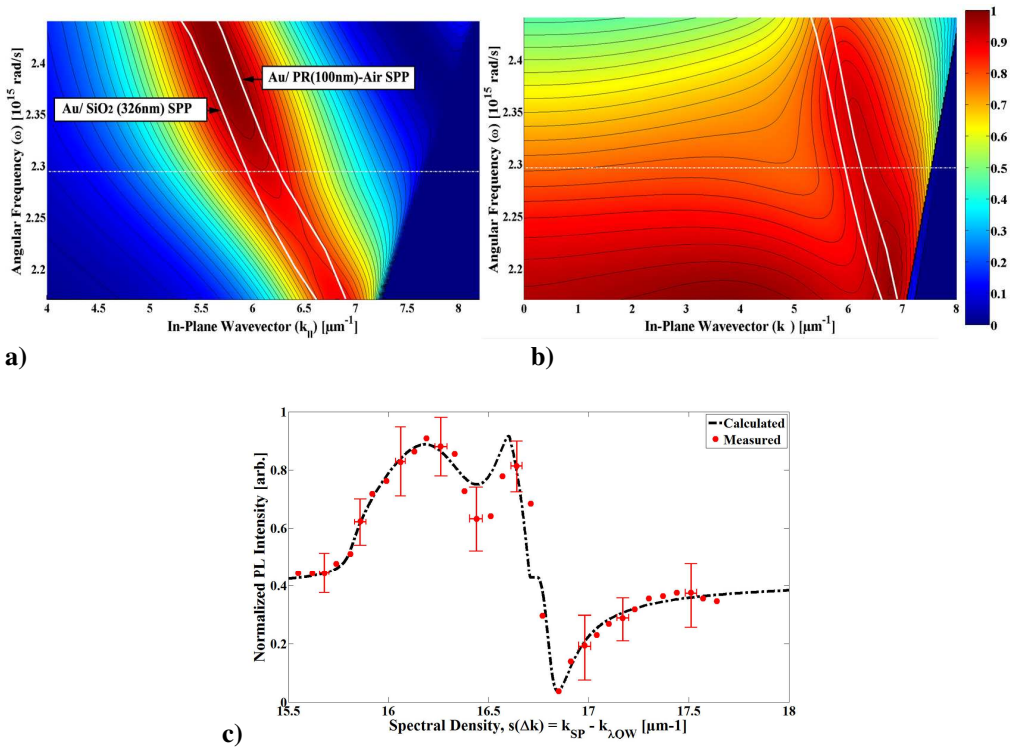

Fig. 3. (a) Calculated dispersion relation $\omega(k_{ll})$ for the GaAs-AlGaAs architecture in the 1st diffraction order as observed in the far-field in P-Polarization. White lines follow the analytical SPR peaks from the Au/ SiO_2 (326nm) SPP and the Au/ PR (100nm)-Air SPs. Fig. 3(b) shows the calculated PL intensity in the far-field in P-Polarization with all diffraction orders summed. Intensities are not modulated by QW PL spectra but still normalized to one. Fig. 3(c) compares the measured normalized difference in total QW PL signal [3] with the predicted signal as calculated.

The solid lines follow the diffracted SPP peaks in the 1st diffraction order. The 100nm thick PR layer between the Au and Air layers has a dielectric constant greater than that of SiO_2 for the investigated emission energies. Still, because of the layer thickness and proximity of the dielectric values, the two extracted SPs intensities overlap. This produces a single observable PL peak, which is the effective superposition of the two SPs (from the Au/ PR and the Au SiO_2 interfaces). The resulting peak broadness (full width half maximum) of the SPs in $\omega(k_{ll})$ is large. This is explained by the SPs overlapping and the small metal thickness (10 nm). The relation between metal thickness and SPR peak quality factor is a known effect well covered in literature [2, 13].

Figure 3(b) presents the total transmitted intensity of the architecture in the Far-field, including all diffraction orders. The SPs peaks are still highlighted with the solid white lines. The 0th diffraction order has a relative maximum in transmission in P-Polarization close to total internal reflection (TIR), at Brewster's angle, which shifts the total PL maxima away from the SPR peaks of Fig. 3(a) slightly. The dashed line in Fig. 3(b) is a cross-section at 820nm, corresponding to the investigated QW emission peak. The calculated (dashed black line) and measured (red dots) relative PL intensities for all the diffraction orders are presented in Fig. 3(c). The PL signal from the $1mm^2$ grating region has been normalized with an equivalent surface area outside the grating in the P-Polarization $[(PL_{OUT} - PL_{IN})/ PL_{OUT}]$, as in [3]. In Fig. 3(c), the abscissa shows the spectral density function, thus presenting the system's wavevector injection. The absolute minimum corresponds to the extracted SPR peak (from Au/ PR and Au/ SiO_2), with a spectral density response at the grating's wavevector

#111139 - $15.00 USD Received 8 May 2009; revised 2 Jun 2009; accepted 3 Jun 2009; published 5 Jun 2009

16.89μm^{-1}. The relative minimum between 16.0 μm^{-1} and 16.5μm^{-1} is a mathematical artifact from the subtraction of the two PL signals observed for both measured and calculated data. The correlation between the calculated and measured data is excellent in this Fig. The photonic interactions at various in-plane wavevectors, including the SPs generation and extraction, are easily identified in both the calculations and measurements, which gives practical information for future designs. On the other hand, for these measurements, conclusions should only be drawn on trends given the relatively large uncertainties from the gathered experimental data. These uncertainties come from the standard deviation of the PL signal inside the 1mm^2 grating. Important standard deviations in PL intensity and measured in-plane wavevectors are mainly due to i) the large NA of the PL system and mechanical goniometric measurements and ii) deviations in the grating structure over the 1mm^2 region due to the extended e-beam lithography (6 hours for the 1mm^2 area). Nonetheless, a very strong SPs coupling is observed in the architecture, specifically due to the QW light source. This is caused by the nature of the semiconductor material, as will now be exposed.

3. Grating diffraction and surface plasmon coupling

Recall that SPs of a given metal-dielectric interface always have a greater in-plane wavevector than free propagating light in the medium ($k_{SP} \geq k_{ll}$) [2], thus the use of a prism in classical configurations to couple SPs. For a fixed energy, the SP mode at the Au/Si-NCs interface discussed in Fig. 2 has a lower in-plane wavevector than the SP mode at the Au/PR interface. Therefore, the dielectric values of the source (ε_{Source}) are equal to those of the first material at the interface, ε_{d1} (Si-NCs as well), and lower than the PR's ε_{d2} ($\varepsilon_{d2} > \varepsilon_{d1} \geq \varepsilon_{Source}$). Because the SPs wavevectors are strictly greater than $k_0\varepsilon_{Source}$ ($k_0 \equiv 2\pi/\lambda_{Source}$), no SPs can be coupled in the 0th diffraction order at any of these interfaces. This is because the in-plane wavevector (k_{ll}) emitted by the integrated source (Si-NCs) can never meet the SPs wavevectors (k_{SP}) at the Au/Si-NCs or Au/PR interfaces ($k_{SP2} > k_{SP1} > k_0\varepsilon_{Source}$). Clearly, the SPs can only couple through the ±1st (and greater) diffraction orders where $k_{SP} = k_{ll} \pm n.k_G$ can be met (with n being the diffraction order and k_G the grating's wavevector). The observed SPs coupling power (translated into extracted PL intensity) is weak because it relies entirely on the grating efficiency to transfer power from the 0th order into the ±1st, which is poor for symmetrical gratings having a sinusoidal geometry. The transfer power is also weak in the second investigated architecture (GaAs-QW source) with the square grating. But, in this case, the relation between the dielectrics supporting the SPs is different: $\varepsilon_{GaAs} = \varepsilon_{Source} > \varepsilon_{d2} \approx \varepsilon_{d1}$. The two SPs modes are coupled in the 0th diffraction order, and also in the higher orders (±1, ±2, etc.), because the k_{ll} from the source can always meet k_{SP} ($k_{SP1} < k_{SP2} < k_0\varepsilon_{Source}$). This is possible because for an uncollimated light source, where any point of the interfaces is exposed to the whole range of wavevector spectra, the SPs conditions at the two interfaces can be fulfilled for all the diffraction orders, including the 0th.

The overall intensity of PL emission observed for the two cases investigated here will be influenced by the diffraction, the metal thickness and obviously the power of the integrated light source (excitation conversion efficiency). Nonetheless, the disposition of the dielectrics in the architecture will also strongly influence the coupling efficiency of SPs. We have established that for integrated transmission setup, the SPs diffraction is the targeted signal to be measured for surface probing. That is, the reflected luminescence is returning to the substrate (and is absorbed or lost in heat) and, since the SPs are always past TIR in the architectures, they have to be diffracted in some ways in order to be measured in the Far-field. This signal is inevitably intertwined with the 0th diffraction order, which can be influenced by the photonic architecture, but doesn't present surface sensitive features by itself. Thus, by defining the S/N ratio as the diffracted SP signal divided by the 0th order (considered here as "noise"), we can compare architectures measurabilities at fixed conditions (independent of total transmission power). Figure 4 presents the S/N PL amplitude for three different setups.

#111139 - $15.00 USD Received 8 May 2009; revised 2 Jun 2009; accepted 3 Jun 2009; published 5 Jun 2009

The solid (red) line represents the case where $\varepsilon_{d2} > \varepsilon_{d1} \geq \varepsilon_{Source}$, which corresponds to the conditions met with the Si-NCs setup [8]. Because the SPs are only coupled through the $\pm 1^{st}$ orders, the diffracted signal is weak relative to the background PL mainly represented by the 0^{th} order. Thus, the measurements of such a signal require sensitive instrumentation. The dashed (green) line represents the case where $\varepsilon_{GaAs} = \varepsilon_{Source} > \varepsilon_{d2} \approx \varepsilon_{d1}$, which corresponds to the conditions met with the QW-SPR setup [3]. The S/N ratio is up to 100 times stronger in this case, since all SPs are coupled through the 0^{th} and higher orders. The two SPs are overlaping in one peak. For a resolution in SPs peaks, a third architecture is presented by the dotted (blue) line, where Si_3N_4 replaces SiO_2 and Air replaces the PR in the QW architecture [3] (now with a 40nm thick gold layer), so $\varepsilon_{GaAs} = \varepsilon_{Source} > \varepsilon_{d2} > \varepsilon_{d1}$. All SPs are still coupled through the 0^{th} order, but a significantly better resolvable SPR peak has been achieved in this case.

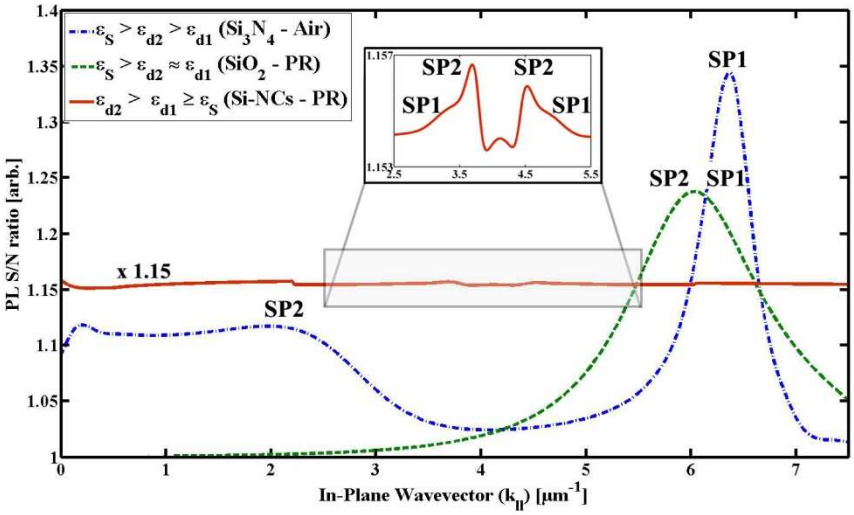

Fig. 4. S/N ratio in total PL for different architectures taken at λ=820nm: In solid red is the Si-NCs setup with $\varepsilon_{d2} > \varepsilon_{d1} \geq \varepsilon_{Source}$, in dashed green is the QW setup with $\varepsilon_{Source} > \varepsilon_{d2} \approx \varepsilon_{d1}$ and in dash-dotted blue is a QW setup with $\varepsilon_{Source} > \varepsilon_{d2} > \varepsilon_{d1}$. SP1 corresponds to the exposed surface (Air or PR) and SP2 to the enclosed interface (Si-NCs, SiO_2 or $Si3N_4$). The solid red line is multiplied by 1.15 for clarity.

As demonstrated, coupling through the 0^{th} order always results in stronger PL modulations (for symmetric gratings) and thus, for a given source power and grating structure, only the Au thickness is left to be optimized for the desired application and measurement system (which sets a minimum in the readable transmission power). Evidently, for symmetric grating structures, it is not possible to reference the measured PL signal to its 0^{th} diffraction order because of intensity intermixing. However, it is possible to simultaneously measure PL outside the grating region on a monolithically integrated SPR device. While this won't equal the 0^{th} order exactly, it can still be used as a reliable reference to contrast the extracted SPs peaks in the total PL coming from the grating region.

In conclusion, we have implemented the Rigorous Coupled-Wave Analysis algorithm combined with the scattering matrices approach to provide a detailed description of the formation and propagation of surface plasmons at metal-dielectric microstructures deposited atop light emitting semiconductor substrates. The calculations have enabled us to predict both the far-field and near-field SP-assisted PL emissions. For symmetric square or sinusoidal gratings, SPs coupling was found to be up to 100 times stronger when all SPs are coupled in the 0^{th} diffraction. An excellent agreement has been observed between calculated and measured experimental results. This understanding allowed us to highlight the specific role of

#111139 - $15.00 USD Received 8 May 2009; revised 2 Jun 2009; accepted 3 Jun 2009; published 5 Jun 2009

semiconductors as light sources for monolithically integrated SPR systems. The explicit conditions established for monolithic SPR represent a fundamental step towards designing a fully integrated quantum semiconductor SPR biosensing device.

Acknowledgments

The authors acknowledge the financial contribution from the Natural Science and Engineering Research Council of Canada (Strategic grant STPGP 350501 - 07) and the Canada Research Chair in Quantum Semiconductors Program.

#111139 - $15.00 USD Received 8 May 2009; revised 2 Jun 2009; accepted 3 Jun 2009; published 5 Jun 2009